Available online at www.sciencedirect.com

jmr&t Journal of Materials Research and Technology

journal homepage: www.elsevier.com/locate/jmrt

Original Article

Durability of TiAl based surface acoustic wave devices for sensing at intermediate high temperatures

Marietta Seifert[*], *Barbara Leszczynska*, *Robert Weser*, *Siegfried Menzel*, *Thomas Gemming*, *Hagen Schmidt*

Leibniz Institute for Solid State and Materials Research Dresden (IFW Dresden), Helmholtzstr. 20, 01069 Dresden, Germany

ARTICLE INFO

Article history:
Received 12 December 2022
Accepted 10 February 2023
Available online 16 February 2023

Keywords:
TiAl IDTs
High-temperature
Surface acoustic wave device
CTGS
aluminum alloy

ABSTRACT

TiAl based surface acoustic wave (SAW) devices, which offer a promising cheap and easy to handle wireless sensor solution for intermediate high temperatures up to 600 °C, were prepared and investigated with respect to their durability. To obtain the devices, Ti/Al multilayers were deposited on high-temperature stable piezoelectric catangasite (CTGS) substrates and structured as electrodes via the lift-off technique. AlNO cover layers and barrier layers at the substrate site served as an oxidation protection. The devices were characterized regarding their electrical behavior by ex-situ measurements of their frequency characteristics after heat treatments up to 600 °C in air. In addition, long-term in situ measurements up to 570 °C were performed to analyze a possible drift of the resonant frequency in dependence on the temperature and time. Scanning electron microscopy of the surfaces of the devices and scanning transmission electron microscopy of cross sections of TiAl interdigital transducer electrode fingers and the contact pads were conducted to check the morphology of the electrode metallization and to reveal if degradation or oxidation processes occurred during the heat treatments.

The results demonstrated a sufficient high-temperature stability of the TiAl based devices after a first conditioning of system. A linear dependence of the resonant frequency on the temperature of about −37 ppm/K was observed. In summary, the suitability of TiAl based SAW sensors for long-term application at intermediate temperatures was proven.
© 2023 The Author(s). Published by Elsevier B.V. This is an open access article under the CC BY license (http://creativecommons.org/licenses/by/4.0/).

1. Introduction

There is strong need in industry for measurement systems working at high temperatures to control devices or component parts and to optimize processes. Especially, systems, which allow a wireless interrogation, are required to access locations, which cannot be reached by wired sensor devices, e.g., on rotating parts. Surface acoustic wave (SAW) based sensors are promising candidates for this field of

* Corresponding author.
E-mail address: marietta.seifert@ifw-dresden.de (M. Seifert).
https://doi.org/10.1016/j.jmrt.2023.02.070
2238-7854/© 2023 The Author(s). Published by Elsevier B.V. This is an open access article under the CC BY license (http://creativecommons.org/licenses/by/4.0/).

application and have therefore been in the focus of research since several years.

A SAW sensor is composed of a piezoelectric, typically single crystalline substrate, on which electrodes in the form of at least one interdigital transducer are present. This system is connected to a matched antenna to realize the wireless interrogation.

There is literature describing SAW sensors working at high temperatures up to about 1000 °C and above [1–8]. In these devices, the electrodes are usually made of Pt or other noble metals, which makes them very expensive and therefore unattractive for common industrial application. However, there are many potential fields for the application of high-temperature sensors, in which the operation temperature is within an intermediate high-temperature regime between 300 °C and 600 °C. To access these temperatures, noble metal based systems are not absolutely required. This temperature regime can be reached using a smart combination of cheap standard materials, which are already used for electrodes in devices working at room temperature or at slightly increased temperatures. In this paper, we suggest the combination of aluminum and titanium in form of the intermetallic TiAl alloy. Aluminum is a standard material for room temperature SAW devices and especially highly-textured Al films or the combination of thick Al layers with thin Ti layers were investigated to achieve a high power durability in early work [9–11]. In contrast to this, we now focus on the intermetallic γ-TiAl phase with its improved high-temperature stability. The low costs and the easy preparation make this material system a very promising candidate for industrial application.

In former work, we investigated the high-temperature behavior of extended TiAl films [12–14] and we showed that TiAl based SAW devices with AlNO cover and barrier layers possessed a long-term high-temperature stability up to at least 500 °C and a short and mid-term stability up to 600 °C [15], which can be further extended by an improved deposition of the cover layer onto the edges of the electrodes. As in the former work, we used single crystal catangasite ($Ca_3TaGa_3Si_2O_{14}$, CTGS) as the piezoelectric substrate because of its superior high temperature stability and promising material properties, which have been extensively investigated in the recent years [16–19].

In this paper, we present a comprehensive analysis of TiAl based SAW devices regarding their electrical characteristics by means of both, ex-situ and temperature dependent in situ measurements, in combination with analyses of the temperature-driven evolution of the morphology of the electrode metallization.

2. Experimental section

The TiAl based electrode structures of one-port resonator designs were realized via a lift-off procedure and the deposition of a stack of alternating Ti and Al layers by e-beam evaporation with an individual layer thickness of 10 nm and a total thickness of 200 nm. Former work showed that the desired high-temperature stable γ-TiAl phase was not formed in co-deposited thin films, whereas it was formed during the annealing of multilayer thin films [13,14]. In the first step, the lift-off mask was prepared on top of the CTGS substrate. An AlNO layer with a thickness of 20 nm prepared by magnetron sputtering was applied as a barrier layer prior to the deposition of the metal layers. Details on the preparation of such films were described in [14].

The structured SAW device, which was obtained after the lift-off procedure, was finally covered with a 40 nm thick AlNO protection layer. Subsequently, a formation annealing of the samples was performed at 600 °C in UHV (base pressure $1.1 \cdot 10^{-9}$ mbar) for 10 h to initiate the interdiffusion of the multilayers and the formation of the desired γ-TiAl phase.

The morphology and possible degradation of the electrode structures were analyzed with scanning transmission electron microscopy (STEM, Technai F30, FEI company, Hillsboro, OR, USA) in combination with energy dispersive X-ray spectroscopy (EDX, Octane T Optima, EDAX Company, Mahwah, NJ, USA). The surfaces of the SAW devices were imaged with scanning electron microscopy (SEM, Zeiss Ultra Plus, Carl Zeiss Microscopy GmbH, Oberkochen, Germany GmbH).

The electrical behavior was characterized via S-parameter measurements with vector network analyzers (VNA, Keysight E5080B and E5071D). Additionally, to monitor the frequency shift during the thermal treatments, in situ electrical measurements were carried out using a Linkam HFS 600 E-PB4 Heating and Freezing Stage with a T95-LinkPad controller (Linkam Scientific Instruments, Salfords, United Kingdom) in air up to 570 °C. Details of the measurement setup and principle were described in [20]. The temperature at the sample position was calibrated with external measurements.

3. Results

3.1. *Morphology of the SAW devices in the as-prepared state and after the formation annealing*

STEM images of TiAl based interdigital transducer finger electrodes in the as-prepared state and after the formation annealing in UHV at 600 °C for 10 h are depicted in Fig. 1. In the as-prepared state (Fig. 1a and b), the sequence of the Ti and Al multilayers was clearly visible. In the image with the predominant element contrast (Fig. 1a), the Ti layers appeared bright, while the Al layers were darker. The first dark layer on top of the CTGS was the AlNO barrier layer. Due to the deposition via magnetron sputtering, the thickness of this layer was reduced at the edges of the lift-off mask. In contrast to this, the metal layers were prepared by e-beam evaporation, which resulted in a more oriented deposition and did not lead to such an effect. The different deposition methods also led to a larger width of about 100 nm of the AlNO layer at both sides of the electrode as compared to the metallic layers. It can be seen that the first Ti layer deposited on top of the AlNO had a very smooth surface. The subsequent Al layer, however, already showed a significant roughness.

The image with the predominant orientation contrast (Fig. 1b) revealed that obviously there was a correlation between the crystal orientation during the growth of the multilayers. Column-like structures throughout multiple layers or across the whole layer stack with grain boundaries along the growth direction were present.

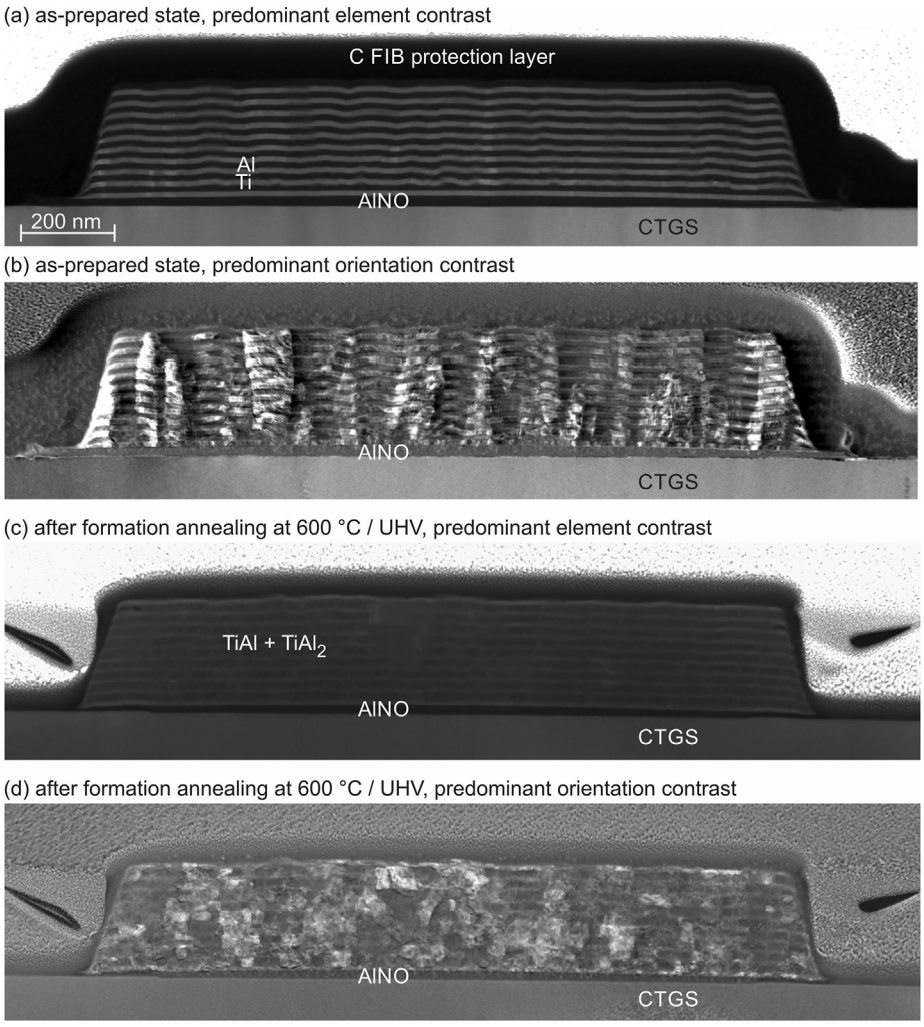

Fig. 1 – STEM images of the TiAl based finger electrode in (a), (b) the as-prepared state without cover layer and (c), (d) after the formation annealing in UHV at 600 °C for 10 h with AlNO cover layer. (a), (c): images with predominant element contrast; (b), (d) images with predominant orientation contrast.

During the formation annealing of the samples at 600 °C in UHV, an interdiffusion of the metal layers took place. However, a fully homogeneous distribution of the material was not reached (Fig. 1c). An EDX evaluation of the different layers revealed that the brighter ones had a composition close to that of the TiAl-phase, while the darker layers had a composition which corresponded to the $TiAl_2$-phase. A layered structure was also still visible in the image with predominant orientation contrast (Fig. 1d).

3.2. *Electrical behavior and morphology of SAW devices with uncovered contact pads*

In order to measure the electrical properties of samples with 40 nm AlNO cover layer, a part of the contact pads was covered with the photoresist prior to the deposition of the AlNO cover layer. Afterwards, the resist was removed via the lift-off procedure, so that the finger structures of the SAW device were protected by the AlNO layer, while the contact pad windows remained uncovered to allow wire bonding. In the first step, the electrical behavior of these samples was measured after the formation annealing at room temperature (RT). Then, the samples were thermally loaded at 400 °C in air for 10 h and then characterized. Subsequently, these samples underwent a second thermal loading at 500 °C in air and were measured again. These heat treatments were performed in a tube furnace with a maximum temperature capability of 1000 °C (Ströhlein Instruments, Viersen) with an Eurotherm 808 controller.

Fig. 2 shows the electrical characteristics of such a SAW device measured at room temperature after the formation annealing and after the two subsequent thermal loadings in air. After the formation annealing, a resonance frequency of 434.6 MHz was detected. After thermal loading at 400 °C in air, the resonance frequency was reduced by about 0.1 MHz, while the subsequent thermal loading at 500 °C led to a further reduction of about 0.3 MHz. This frequency shift was ascribed to oxidation processes in the open TiAl contact pad regions. Since there was no cover layer, the heat treatment in air led to a partial oxidation of the TiAl which changed the electrical resistivity within the contact pad and finally resulted in the shift of the resonant frequency.

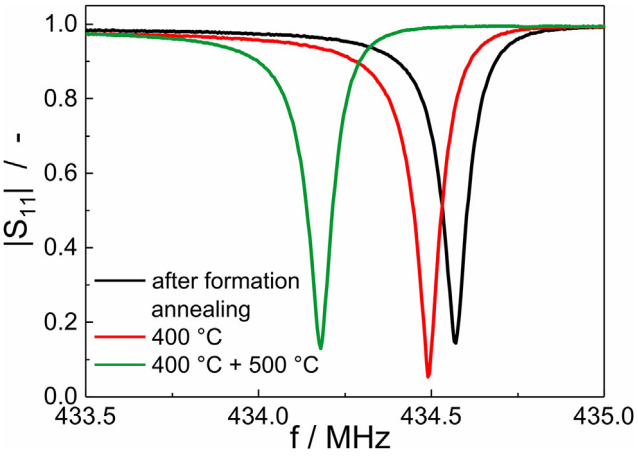

Fig. 2 – Electrical characteristics in terms of the reflection coefficient $|S_{11}|$ of a SAW device without AlNO cover layer at the contact pads after the formation annealing in UHV (600 °C, 10 h) and after thermal loading in air for 10 h at 400 °C and subsequently at 500 °C.

The temperature dependent resonant frequency of a sample without an AlNO cover layer on the pads measured in situ with the Linkam stage is shown in Fig. 3a. The temperature of the sample was increased stepwise from 25 to 550 °C. All temperature steps and dwell times are summarized in Table 1. The resonant frequency was first recorded as soon as the respective temperature was reached and a second time after the dwell time, which are the values presented in this paper. After thermal loading at the maximum temperature of 550 °C, the sample was cooled down and the frequencies were recorded when the respective temperatures were reached without further dwell times. All values shown in the figures are normalized to the frequency measured at RT prior to the thermal loading.

As expected from literature [21], the measurement curves revealed an almost linear decrease of the resonant frequency with increasing temperature. From a linear fit, the 1st order temperature coefficient was deduced as −37.1 ppm/K. Fig. 3c presents the frequency drift Δf normalized to the frequency measured at RT, which was caused by irreversible changes of morphology during the dwell time at the respective temperature listed in Table 1. It can be seen that for temperatures below 380 °C, the frequency did not change during the thermal loading at the respective temperature. In contrast to this, during the thermal loading at 550 °C, the frequency decreased irreversibly by 0.16 MHz, which corresponded to a value of $\Delta f/f_{25°C} = 0.33 \cdot 10^{-3}$. During the subsequent cooling of the sample, this offset remained almost constant with respect to the frequencies measured during the heating up, leading to a parallel course of the cooling down curve leaving behind a small irreversible frequency shift of 0.23 MHz at 50 °C.

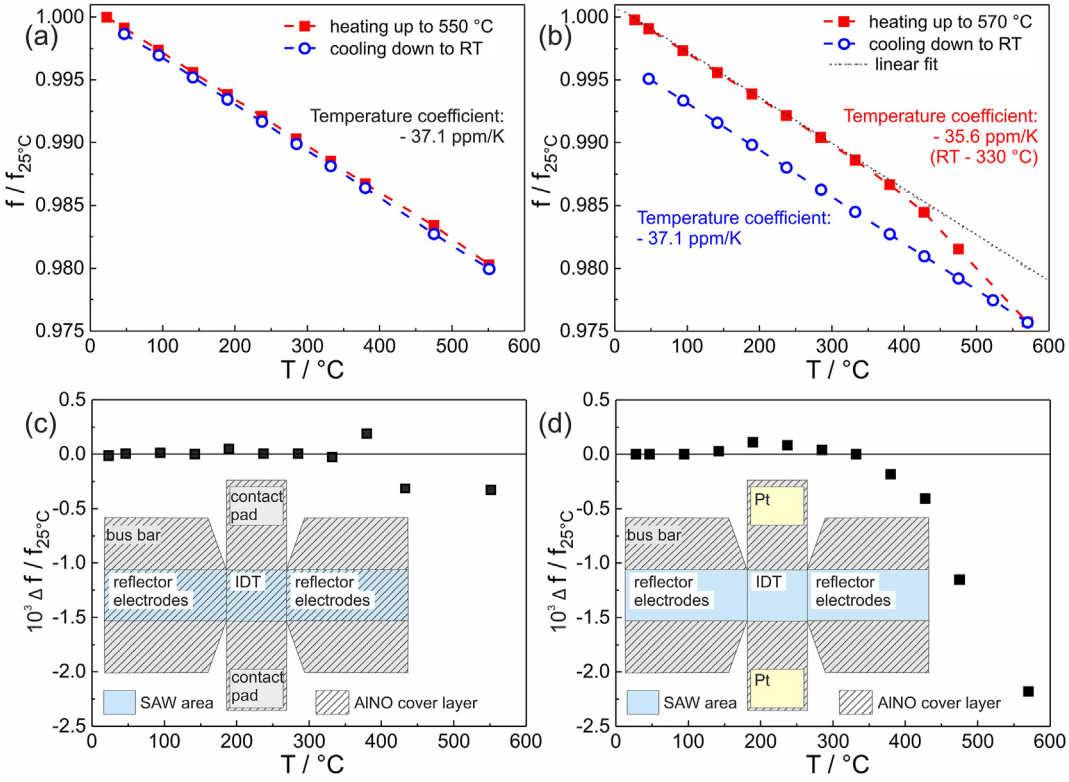

Fig. 3 – In situ measured normalized resonance frequency in dependence on the temperature during heating and cooling of the sample: (a) SAW device without AlNO cover layer on the contact pads, (b) SAW device without AlNO cover layer on the electrode fingers. The dashed lines serve as guide to the eye. (c) and (d) demonstrate the normalized frequency drift $10^3 \cdot \Delta f/f_{25°C}$ of (a) and (b) during the dwell time at the respective temperature. The insets in (c) and (d) demonstrate the architecture of the SAW device and the distribution of the AlNO cover layer.

Table 1 – Temperature steps and dwell times used for the measurement of the sample without AlNO cover layer at the contact pads of the SAW device (Fig. 3a,c).

T/°C	25	45	95	140	190	235	285	330	380	475	550
dwell time/h	2	56	24	28	20	5	19	24	72	72	24

Fig. 3b summarizes the normalized temperature dependent course of the resonant frequency measured for a sample, in which the finger electrodes were not protected with the AlNO cover layer. In this case, the contact pad windows without the AlNO protection layer were covered with a 150 nm thick Pt layer. The shift of the resonance frequency of the sample was measured in the Linkam stage during thermal loading up to 570 °C. The temperature steps and dwell times are summarized in Table 2. The corresponding frequency values measured after each dwell time are shown in the plot. As before, the sample was cooled down without further dwell times and the frequencies were recorded when the respective temperatures were reached.

In contrast to the sample with the cover layer on the finger electrodes, the decrease of the resonance frequency was enhanced above a temperature of 380 °C. A linear fit of the measured results up to 330 °C revealed a slope of 36.5 ppm/K. In Fig. 3d, the normalized frequency drift $\Delta f/f_{25°C}$ during the annealing at the respective temperatures is shown. It can be seen that above 380 °C, Δf was much larger as compared to the sample with covered finger electrodes (Fig. 3c).

During the cooling down, which was performed without any dwell times at the measurement temperatures, a linear increase of the resonance frequency was observed with a slope of −37.1 ppm/K, which was the same as measured for the sample with cover layer. This finding is reasonable, since the temperature coefficient is mainly determined by the substrate properties, while the electrodes only have a minor influence on this value. In addition, the cooling was performed without any dwell times at the respective temperatures, so that any further changes leading to a further irreversible drift of the resonant frequency, could hardly occur within the electrodes. In summary, this behavior resulted in an about 1.8 MHz lower resonant frequency value of the sample remeasured at room temperature as compared to the state prior to the thermal loading procedure.

Fig. 4 compares STEM images of a finger electrode with cover layer (Fig. 4a) and without cover layer (Fig. 4b) after the annealing procedures. For both samples, the layered structure, which was visible after the formation annealing (Fig. 1), was not present any more after the thermal loading in air. In case of the covered finger (Fig. 4a), only a minor oxidation occurred close to the edges. EDX measurements proved that the dark contrast at these positions in the image with predominant element contrast originated from Al_2O_3 grains. In the image with the predominant orientation contrast, an irregular grain structure was present with several large grains with a size up to 200 nm and many smaller grains with sizes of a few up to a few tens of nm. In contrast to this, a small amount of oxygen was found almost everywhere within the finger without cover layer (Fig. 4b). Just in the center of the finger, no oxygen was detected. In addition, the grains were much smaller. Only very few larger grains with sizes of 50–100 nm were present. The surface of the finger consisted of layered TiO_2 and Al_2O_3 with a significantly larger roughness as compared to the film with cover layer.

The shift of the resonance frequency in case of the samples with the uncovered contact pad was negligible as compared to the device with the uncovered electrodes. The reason for the different impact of the oxidation of the electrodes and the contact pads on the frequency behavior is the strong influence of changes of the finger electrodes due to oxidation regarding their mechanical properties, like stiffness and elastic modulus, as well as the density and thickness on the acoustic behavior of the IDT and reflectors. In contrast to this, changes within the contact pads indeed change the overall electrical resistance; however, hardly influence the acoustic properties in the active area of the devices, leading to only small changes of the frequency.

In summary, the findings emphasize the necessity of an oxidation protection, especially of the electrode structures.

3.3. *Electrical behavior and morphology of SAW devices with covered pads*

In a second experiment, again samples, in which the electrode fingers of the SAW device were protected with the AlNO cover layer, were investigated. However, in this case, the area, in which the AlNO cover layer was removed at the bond pads, was now locally covered with a 150 nm thick Pt layer. This layer, which was added after the formation annealing, was required to facilitate the Pt wire bonding in the in situ measurement setup and simultaneously covered the free surface of the TiAl. These devices with the formation-annealed TiAl layer and as-deposited Pt layer will be called as-prepared SAW chip in this section. The samples were thermally loaded stepwise at 400, 500 and 600 °C and for each state the electrical characteristics in terms of the reflection coefficient $|S_{11}|$ was measured afterwards at room temperature, showing the resonance peak of about 433 MHz. Fig. 5 summarizes these results. After the thermal loading at 400 and 500 °C, the resonance frequency increased by 0.2 MHz and by further 0.4 MHz, respectively. This was in contrast to the sample with the uncovered pads, where a decrease in frequency was

Table 2 – Temperature steps and dwell times used for the measurement of the sample without AlNO cover layer at the fingers of the SAW device (Fig. 3b,d).

T/°C	30	45	95	140	190	235	285	330	380	425	475	570
dwell time/h	0.1	0.1	0.1	15	37	48	46	8	24	72	113	24

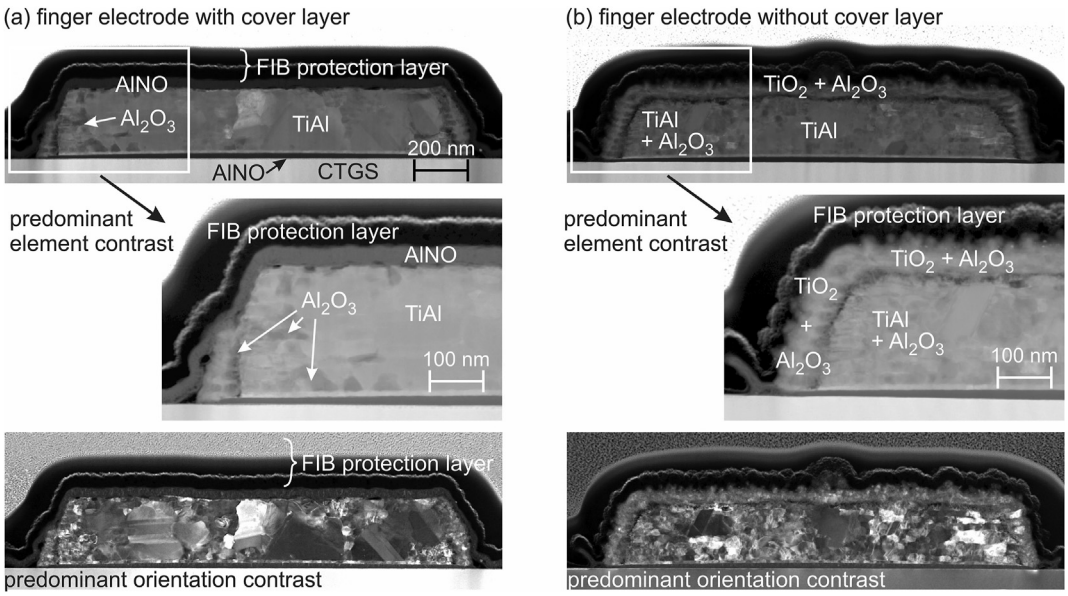

Fig. 4 – STEM images of a finger electrode (a) with cover layer and (b) without cover layer after the annealing procedure listed in Table 2. In the top row, images with predominant element contrast, in the bottom row with predominant orientation contrast are shown. The enlarged images with enhanced contrast clarify the difference in degradation and roughness.

observed at these temperatures. The thermal loading at 600 °C led to a decrease of the resonance frequency of 0.8 MHz, which corresponded to a decrease of 0.2 MHz as compared to the value measured for the as-prepared SAW chip.

Figs. 6 and 7 present STEM images of an electrode finger of such a SAW device and of a contact pad with the Pt layer after the complete thermal loading procedure. The image of the electrode finger with predominant element contrast (Fig. 6a) shows that also for these samples, the layered structure, which was observed after the formation annealing, was not present any more. Hardly any oxidation occurred inside the finger. Solely, at the edges of the finger, TiO_2 was formed. A layer of Al_2O_3 with a thickness of a few nm was present between the TiO_2 and the TiAl.

The image with orientation contrast in Fig. 6b also shows no correlation to the former layer structure. The morphology was irregular with globular and extended grains with grain sizes of a few tens of nm up to more than 100 nm.

Fig. 7a presents an SEM image of the contact pad, which was covered by a Pt layer, after the thermal loading. Due to the heat treatment, locally large Pt grains grew. In the cross section STEM image in Fig. 7b, an about 500 nm large Pt grain is visible. A pore formed between this grain and the layer below. Fig. 7c shows two STEM images with predominant element contrast, which are optimized to visualize the Pt layer and the TiAl layer, respectively. The degradation of the upper region of the metallic layer can be seen. Below the Pt layer, an about 70 nm thick region consisting of a mixture of TiO_2 and Al_2O_3 developed. In addition, in the upper region of the TiAl layer, locally Al_2O_3 grains were present. The Pt layer contained small pores. Some of them were filled with TiO_2.

These results showed that during the annealing of this sample two processes took place. On the one hand side, there was a healing of defects and a crystal growth accompanied by an agglomeration of the Pt layer leading to the large grains and pores. Light microscopy images demonstrated that this process already started at low temperatures of 400 °C. These two different processes of defect healing and agglomeration, which take place within the Pt layer, have an opposing influence on its resistivity and therefore can lead to a change of the resonant frequency of the device depending on their extend within the temperature regimes. During the thermal loading up to 600 °C, there was a diffusion of oxygen through the Pt layer inside the sample and a partial diffusion of Ti into the Pt. The Ti solved in the Pt got oxidized and formed TiO_2. The upper region of the TiAl film below the Pt cover layer became oxidized as well. As in the film with the uncovered contact

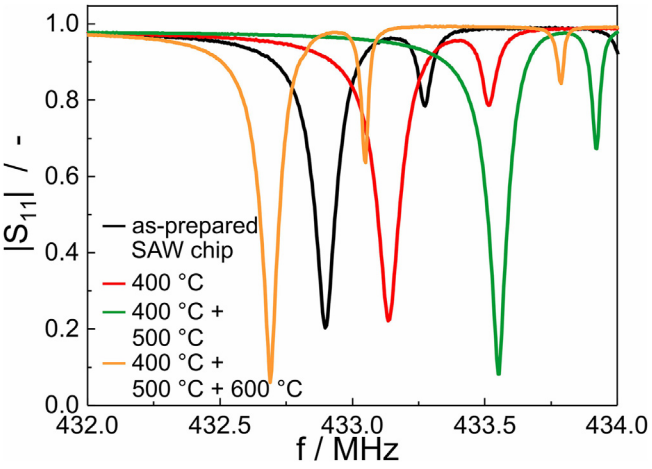

Fig. 5 – Electrical characteristics in terms of the reflection coefficient $|S_{11}|$ of the as-prepared SAW chip with Pt layer on the contact pads measured at RT in the as-prepared state and after thermal loading in air for 10 h at 400 °C, 500 °C and 600 °C.

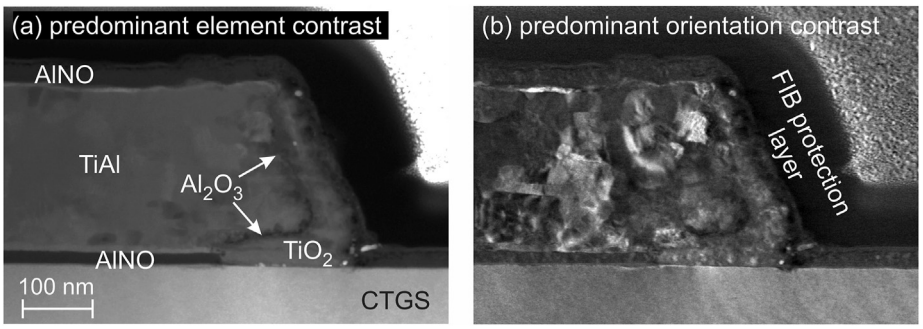

Fig. 6 – STEM images of the TiAl based finger electrode after annealing at 400, 500 and 600 °C in air for 10 h in each case. Image with (a) predominant element contrast, (b) predominant orientation contrast.

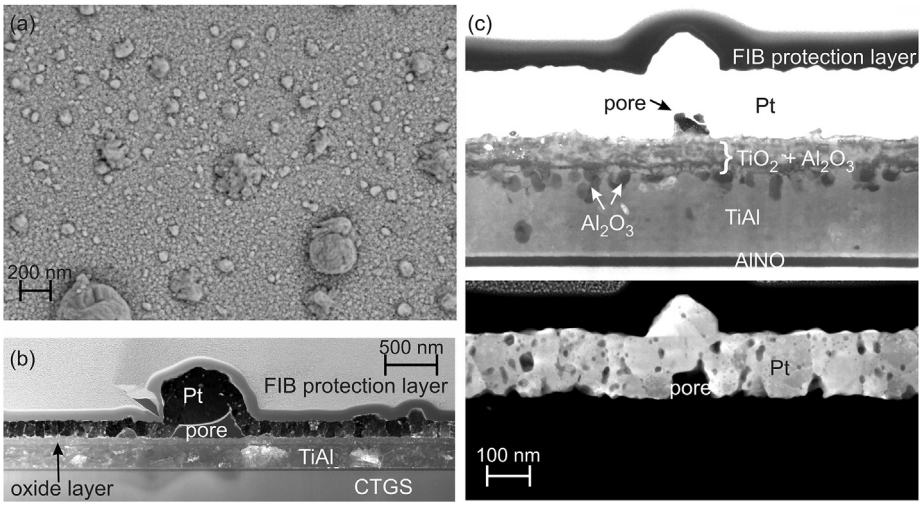

Fig. 7 – Contact pad covered with a Pt layer after thermal loading up to 600 °C: (a) top view SEM image (inLens, 6 kV), (b) cross section STEM image (predominant orientation contrast), (c) cross section STEM images (predominant element contrast) of the same position with different contrast to visualize details in the TiAl and oxide layers (upper image) as well as in the Pt layer (lower image).

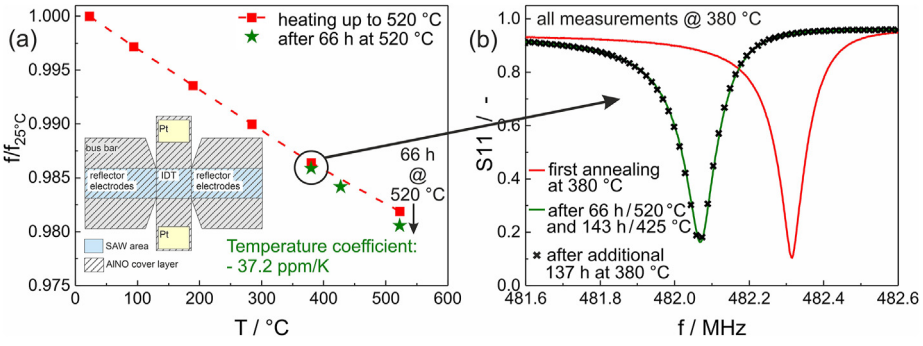

Fig. 8 – Electrical behavior of a sample with AlNO cover layer at the electrodes and a Pt layer at the contact pads: (a) in situ measured normalized resonance frequency in dependence on the temperature during thermal loading of the sample up to 520 °C (red squares) and at individual states during cooling down (green stars). (b) Frequency characteristics in terms of the reflection coefficient $|S_{11}|$, all measured at 380 °C. Red curve: stop at 380 °C during first thermal loading, green curve: after a subsequent thermal loading at 520 °C for 66 h and at 425 °C for 143 h, black crosses: after a further thermal loading at 380 °C for 137 h.

Table 3 – Temperature steps and dwell times used for the measurement of the sample with AlNO cover layer at the electrodes and a Pt layer at the contact pads (Fig. 8).

T/°C	25	95	190	285	380	520	425	380
dwell time/h	0.1	0.1	0.1	0.1	0.1	66	143	137

pads, this oxidation then led to the observed degradation of the device behavior.

Fig. 8a shows the normalized resonance frequency in dependence on the temperature measured for the device with the AlNO cover layer at the electrodes and the Pt layer at the contact pads. The temperature steps and dwell times are summarized in Table 3. Up to 380 °C, the frequencies were recorded as soon as the respective temperature was reached. The sample was then set to 520 °C for 66 h. The resonance frequency was determined as soon as this temperature was reached (red square at 520 °C in Fig. 8a) and after 66 h (green star at 520 °C). Then, the sample was cooled down to 425 °C, hold there for 143 h, and subsequently set to 380 °C (137 h). It can be seen that during the heating of the sample, there was a linear change of the frequency with temperature up to 380 °C. A linear fit led to a slope of −38.0 ppm/K. The first frequency value measured at 520 °C was sligthly larger as expected from the linear course up to 380 °C. As discussed earlier, this increase can be ascribed to changes in the Pt layer. After the dwell time, a slightly lower frequency was observed, which originated from the above described oxidation processes in the sample. The values measured after the dwell time at 520 °C and at the two temperatures during cooling down indicate a linear increase in frequency with a slope of 37.2 ppm/K.

Fig. 8b summarizes the resonance frequency measured at 380 °C after various states of the thermal loading procedures. During the first thermal loading, at 380 °C a resonance frequency of 482.3 MHz was measured (red curve). After the annealing at 520 °C for 66 h and subsequently at 425 °C for 143 h, the resonance frequency measured at 380 °C was reduced to 482.1 MHz (green curve). After another annealing at 380 °C for 137 h, no further shift of the resonance frequency was detected (black crosses). This measurement series demonstrated that during the first thermal loading at higher temperatures (520 °C in this case), a stable state of the sample was reached. Therefore, further heat treatments at the lower temperature of 380 °C did not lead to further changes of the resonance frequency.

4. Conclusions

In this paper, TiAl based SAW devices were investigated regarding their suitability for application at intermediate high temperatures up to 600 °C. The results demonstrate that a conditioning of the as-prepared devices is required to stabilize the morphology. After this conditioning, a stable frequency behavior at intermediate temperatures and a linear shift of the frequency with temperature were observed. These findings confirm the suitability of this cheap and easy to handle material system for use in standard high-temperature applications as, e.g., temperature sensors. Additionally, the high-temperature stability can be further improved by optimizing the cover layer deposition at the edges of the electrode fingers.

Data availability

The raw/processed data required to reproduce these findings cannot be shared at this time as the data also forms part of an ongoing study.

Declaration of Competing Interest

The authors declare the following financial interests/personal relationships which may be considered as potential competing interests: Marietta Seifert reports financial support was provided by German Research Foundation. Marietta Seifert reports financial support was provided by German BMWI. Barbara Leszczynska reports financial support was provided by German BMWI.

Acknowledgements

The work was supported by BMWI (Bundesministerium für Wirtschaft und Energie), Germany (03ET1589 A) and DFG (Deutsche Forschungsgemeinschaft), Germany (470028346).

The authors gratefully acknowledge Andreas Büst for thin film deposition, and Thomas Wiek and Dina Bieberstein for SEM images and TEM lamella preparation.

REFERENCES

[1] Aubert T, Elmazria O, Assouar MB. Wireless and batteryless surface acoustic wave sensors for high temperature environments. 2009 9th International Conference on Electronic Measurement & Instruments; 2009 16-19 Aug. 2009. https://doi.org/10.1109/ICEMI.2009.5274413.

[2] Aubert T, Bardong J, Elmazria O, Bruckner G, Assouar B. Iridium interdigital transducers for high-temperature surface acoustic wave applications. IEEE Trans Ultrason Ferroelectrics Freq Control 2012;59:194–7.

[3] Moulzolf SC, Frankel DJ, da Cunha MP, Lad RJ. High temperature stability of electrically conductive Pt–Rh/ZrO_2 and Pt–Rh/HfO_2 nanocomposite thin film electrodes. Microsyst Technol 2014;20(4–5):523–31.

[4] Liu X, Peng B, Zhang W, Zhu J, Liu X, Wei M. Improvement of high-temperature stability of Al_2O_3/Pt/ZnO/Al_2O_3 film electrode for SAW devices by using Al_2O_3 barrier layer. Materials 2017;10(12):1377.

[5] Taguett A, Aubert T, Elmazria O, Bartoli F, Lomello M, Hehn M, et al. Comparison between Ir, $Ir_{0.85}Rh_{0.15}$ and $Ir_{0.7}Rh_{0.3}$ thin films as electrodes for surface acoustic waves applications above 800 °C in air atmosphere. Sensors and Actuators A: Physical. 2017;266:211–8.

[6] De Sousa Lopes Moreira A, Bartasyte A, Belharet D, Soumann V, Margueron S, Broenner A. Stabilized Pt interdigitated electrodes for high-temperature SAW sensors. 2021 IEEE International Ultrasonics Symposium (IUS); 2021 11-16 Sept. 2021.

[7] Zhou X, Tan Q, Liang X, Li B, Guo T, Gan Y. Novel multilayer SAW temperature sensor for ultra-high temperature environments. Micromachines 2021;12(6):643.

[8] Xue T, Xu F, Tan Q, Yan X, Liang X. LGS-based SAW sensor that can measure pressure up to 1000 °C. Sensors and Actuators A: Physical. 2022;334:113315.
[9] Weihnacht M, Menzel S, Wetzig K. In: Wetzig K, Schneider CM, editors. Metal based thin films for electronics, vol. 28. Wiley; 2006. p. 261.
[10] Matsukura N, Kamijo A, Ootsuka E, Takahashi Y, Sakairi N, Yamamoto Y. Power durability of highly textured Al electrode in surface acoustic wave devices. Jpn J Appl Phys 1996;35(5S):2983.
[11] Hofmann M, Gemming T, Wetzig K. Microstructure and composition of annealed Al/Ti-metallization layers. Anal Bioanal Chem 2004;379(4):547–53. https://doi.org/10.1007/s00216-004-2619-9.
[12] Lattner E, Seifert M, Gemming T, Heicke S, Menzel SB. Coevaporation and structuring of titanium–aluminum alloy thin films. J Vac Sci Technol: Vacuum, Surfaces, and Films 2017;35(6):061603. https://doi.org/10.1116/1.4999565.
[13] Seifert M, Lattner E, Menzel SB, Oswald S, Gemming T. Phase Formation and high-temperature stability of very thin Co-sputtered Ti-Al and multilayered Ti/Al films on thermally oxidized Si substrates. Materials 2020;13(9):2039. https://doi.org/10.3390/ma13092039.
[14] Seifert M, Lattner E, Menzel S, Oswald S, Gemming T. Study of TiAl thin films on piezoelectric CTGS substrates as an alternative metallization system for high-temperature SAW devices. J Mater Res Technol 2021;12:2383–95. https://doi.org/10.1016/j.jmrt.2021.04.006.
[15] Seifert M, Leszczynska B, Menzel SB, Gemming T. Long-term high-temperature behavior of Ti-Al based electrodes for surface acoustic wave devices. J Mater Res Technol 2022;19:989–1002. https://doi.org/10.1016/j.jmrt.2022.04.027.
[16] Suhak Y, Schulz M, Johnson WL, Sotnikov A, Schmidt H, Fritze H. Electromechanical properties and charge transport of $Ca_3TaGa_3Si_2O-14$ (CTGS) single crystals at elevated temperatures. Solid State Ionics 2018;317:221–8.
[17] Biryukov SV, Schmidt H, Sotnikov A, Weihnacht M, Sakharov S, Buzanov O. CTGS material parameters obtained by versatile SAW measurements. 2014 IEEE International Ultrasonics Symposium 2014 3-6 Sept. 2014. https://doi.org/10.1109/ULTSYM.2014.0217.
[18] Suhak Y, Fritze H, Sotnikov A, Schmidt H, Johnson WL. High-temperature electromechanical loss in piezoelectric langasite and catangasite crystals. J Appl Phys 2021;130(8):085102.
[19] Weihnacht M, Sotnikov A, Suhak Y, Fritze H, Schmidt H. Accuracy analysis and deduced strategy of measurements applied to $Ca_3TaGa_3Si_2O_{14}$ (CTGS) material characterization. 2017 IEEE International Ultrasonics Symposium 2017 6-9 Sept. 2017. https://doi.org/10.1109/ULTSYM.2017.8092822.
[20] Weser R, Sotnikov A, Schmidt H. Advanced characterization of surface acoustic wave fields at high temperature. 2018 IEEE International Ultrasonics Symposium (IUS); 2018. p. 1–4. https://doi.org/10.1109/ULTSYM.2018.8579907.
[21] Yang Y, Peng B, Yue H, Huang F, He P, He Z, et al. Temperature characteristics of surface acoustic wave resonators prepared on (0°, 90°, Ψ) CTGS cuts. Applied Acoustics; 2022;194:108788.